machines

MDPI

Article

A Non-Perturbative Framework in Analyzing Weakly Nonlinear Oscillators and Their Chaotic Dynamics

Galal M. Moatimid [1], T. S. Amer [2] and A. A. Galal [3,*]

[1] Department of Mathematics, Faculty of Education, Ain Shams University, Cairo 11517, Egypt; gal_moa@edu.asu.edu.eg
[2] Department of Mathematics, Faculty of Science, Tanta University, Tanta 31527, Egypt
[3] Department of Engineering Physics and Mathematics, Faculty of Engineering, Tanta University, Tanta 31734, Egypt
* Correspondence: abdallah.galal@f-eng.tanta.edu.eg

Abstract

Weakly nonlinear oscillators display complex behavior that perturbation methods struggle to analyze, particularly near critical thresholds. The non-perturbation approach (NPA) offers a unified, parameter-agnostic approach that is effective in strongly resonant situations, accurately capturing global phase space structures, and directly addressing chaotic transitions, providing predictive insights where traditional methods fail. The NPA as a novel technique successfully converts the nonlinear weakly oscillator of the ordinary differential equation (ODE) into a linear issue. Theoretical findings are confirmed through a numerical comparison using Mathematica Software (MS). The results of the numerical solution (NS) show excellent agreement. It is commonly acknowledged that all conventional perturbation methods utilize Taylor expansion to augment restoring forces, hence optimizing the usual conditions. A comprehensive analysis of the issue's stability is easily achievable via NPA. Accordingly, when evaluating NS estimates of weakly nonlinear oscillators, NPA occupations serve as a more useful form of responsibility. Additionally, the stability analysis is easily accomplished via NPA. The system's dynamics are examined by chaotic analyses, incorporating bifurcation diagrams (BDs), Poincaré maps (PMs), and Lyapunov exponents (LEs). This analysis identifies transitions between regular and complicated behavior and thoroughly examines the system's stability features. The results provide a comprehensive understanding of the fundamental nonlinear dynamics and offer significant insights for future research on analogous systems.

Keywords: non-perturbative approach; nonlinear oscillators; stability configuration; bifurcation diagrams; chaos diagnostics

Check for updates

Academic Editor: Dimitrios Giagopoulos

Received: 17 January 2026
Revised: 21 February 2026
Accepted: 23 February 2026
Published: 27 February 2026

Copyright: © 2026 by the authors. Licensee MDPI, Basel, Switzerland. This article is an open access article distributed under the terms and conditions of the Creative Commons Attribution (CC BY) license.

1. Introduction

Nonlinear ODEs are essential in modeling real-world phenomena, as numerous natural and artificial systems have intrinsic nonlinearity. In contrast to linear models, nonlinear ODEs can encapsulate intricate dynamics, including instability, bifurcations, oscillations, and chaos, rendering them indispensable for elucidating phenomena in physics, biology, engineering, economics, and environmental research. Their research offers enhanced understanding of system dynamics and facilitates more precise forecasting and regulation of real-world systems [1–3].

Nonlinear oscillators are increasingly important in mathematics and engineering, as solving nonlinear ODEs is more complex than dealing with linear ones, particularly

regarding force and nonlinear damping. Recent research focuses on developing advanced analytical NSs in analyzing mathematical models across various scientific and engineering domains, highlighting the critical role of nonlinear ODEs in physics, biology, and chemistry. They were involved in resolving issues in dynamical systems, including network mathematics and optimization, as well as engineering challenges related to materials, energy, and electrical infrastructure [4]. The connected technique functions are extraordinarily consistent across the full range of beginning amplitudes and compute higher-order estimates. The implementation of the coupled homotopy-variational method on the nonlinear Duffing oscillator (DO) revealed new frequency–amplitude relationships [5]. The relevant literature clarified the approach in determining the equivalent spring constant of linearly coupled springs in series. A system comprising a mass supported by both a linear spring and a nonlinear spring was examined [6].

A collection of significant oscillators is widely used in physics and engineering and has attracted the interest of many investigators. The Aboodh transform, employing the homotopy perturbation method (HPM), was utilized to obtain an approximate analytical solution of the specified problem [7]. A nonlinear oscillator was enhanced with two significant linear components [8]. The concise report functions as a framework of various applications aimed at establishing the period or frequency of nonlinear oscillators [9]. Hamiltonian method was a logical approximation technique employed to examine extremely nonlinear ODEs [10]. An innovative method combining HPM with a variational formula was formulated to obtain an exact analytical solution of a nonlinear ODE defined by inertia and static nonlinearity [11]. The gained results are compared with alternative analytical and exact responses to illustrate the surprising precision and thoroughness of the approximate analytical method. A novel method of global error minimization is introduced to tackle nonlinear third-order Jerk ODEs, focusing on the identification of unknown parameters up to third order [12].

A variety of improved perturbation techniques, along with other mathematical tools such as vibrational theory, HPM, and iterative strategies, are employed to address limitations of conventional perturbation approaches. Some asymptotic methods of nonlinear ODEs were made in the application of both weak and strong nonlinearities [13]. The project primarily emphasizes Chinese accomplishments in this area. Three evaluations of nonlinear oscillators were conducted employing fundamental techniques: the max–min methodology, HFF, and HPM [14]. The weighted average is utilized to improve the precision of frequency representation in a mathematical model. It was suggested that extremely nonlinear oscillators may be entirely and effortlessly regulated [15]. The results demonstrate that the method produced a largely accurate response. The study provided an effective method of rapidly analyzing the amplitude–frequency relationship of a nonlinear oscillator. An experimental micro-electro-mechanical system and a packaging system employed the correlation between frequency and amplitude in nonlinear vibratory systems and were previously recorded [16]. A direct frequency prediction method is proposed for nonlinear oscillators with initial conditions (ICs), and an effective strategy for comprehending vibrational features of a nonlinear oscillating system is constructed. Recent advancements were showcased in the fields of Fluid Mechanics as well as Dynamical Systems [17–20]. The NPA was successfully modified to investigate the coupled nonlinear ODEs [21–23]. The following details must highlight that the novel approach generates a unique linear ODE that relates to the current nonlinear ODE. The novel method produces a compatible linear ODE that is equivalent to the current nonlinear one, with the following advantages:

1. The novel method is utilized to formulate a new linear ODE that is equivalent to the original nonlinear one.

2. In light of the new technique, there exists a perfect correlation between these two ODEs.
3. This solution effectively resolves the deficiencies in previous techniques.
4. In contrast to other perturbation methods, NPA enables experts to evaluate the stability of a situation with ease.
5. NPA seems to be a direct, promising, and intriguing tool.
6. Further combinations of interconnected Dynamical Systems, considered substantial, efficient, and compelling, may be included in the scope of NPA.
7. Taylor expansion is employed to facilitate the calculation of restoring forces in all classical perturbation methodologies, including a fundamental technique known as the multiple time scales. Furthermore, the NPA disregarded this shortcoming.
8. NPA addresses restoring forces through a methodology that is independent of standard perturbation approaches and does not fall under perturbation methods.

Additionally, the NPA has three significant drawbacks. They can be listed as follows:

1. The methodology relates to a weakly second-order oscillator of ODEs.
2. The fundamental conditions remain unchanged.
3. To attain enhanced precision, the initial amplitude must be below one.

The investigation of NPA in evaluating weakly nonlinear oscillators and their chaotic dynamics possesses substantial experimental and practical importance, as it facilitates the precise definition of complicated phenomena that conventional perturbation methods frequently overlook. This framework is essential in examining systems such as micro- and nano-electromechanical resonators, and nonlinear optical cavities, where weak nonlinearities can result in complex phenomena, including bifurcations, multi-frequency interactions, mode coupling, and chaotic transitions. Utilizing NPA, researchers may forecast and corroborate the complete amplitude-dependent responses, energy transfer mechanisms, and sensitivity to initial conditions evident in laboratory studies, yielding an exact correspondence with real-world dynamics. This methodology has extensive applications in engineering and applied sciences, encompassing the design of vibration control systems, stability of power grids, optimization of chaos-based secure communication systems, and modeling of intricate biological rhythms. The NPA effectively connects theoretical analysis with actual results, providing strong predictions for long-term development, synchronization phenomena, and the emergence of chaos in weakly nonlinear oscillatory ODEs. The following sections of the paper will elaborate on the methods of our investigation in greater detail. Section 2 analyzes two distinct problems as extremely nonlinear ODEs and provides a discussion of the BDs, PMs, and the LEs, as well as further findings, outcomes, and discussions related to stability analysis. Section 3 delineates the foremost key outcomes.

2. Applications

This section aims to investigate two distinct dynamical systems of very strong nonlinearity NPA as previously mentioned [17–19].

2.1. First Application

The first dynamical application is considered as a small block of mass m and is subjected to forces as shown in Figure 1. This block moves smoothly in a straight line. Assuming that the elastic restoring force $F_y = may$, the block will be oscillated under a damping force denoted by $F_D = mcy'$, and a resisting force $F(y) = mby^2 - mhy^3 + mf \sin y$. The latter force is presumed to act to the left. In the context of a weakly nonlinear oscillator, the physical quantities a, b, c, h and f can be interpreted as follows:

a signifies linear stiffness coefficient. It represents the restoring force proportional to displacement y, analogous to the spring constant in a linear oscillator.

b indicates quadratic nonlinearity coefficient. It introduces asymmetry in the restoring force and governs the strength of the term proportional to y^2.

c addresses the damping coefficient. It represents energy dissipation in the system, proportional to the velocity y', and modeling effects such as friction or air resistance.

h indicates the cubic nonlinearity coefficient. It defines the strength of the nonlinear stiffening or softening term proportional to y^3, which can lead to phenomena like amplitude-dependent frequency shifts or bifurcations.

f defines the forcing amplitude. In the $\sin y$ term, it characterizes the magnitude of an external periodic nonlinear forcing applied to the system.

Therefore, the quantities a, b, c, h and f are physical parameters that maintain the force's units of the three previously mentioned forces.

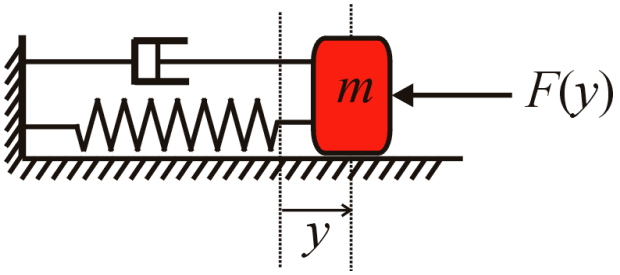


Figure 1. A vibrating block as addressed in the first application.

The governing equation of motion can be formulated as follows:

$$my'' = -F_D - F_y - F(y); \tag{1}$$

where $F_D = mcy'$, $F_y = may$ and $F(y) = mby^2 - mhy^3 + mf \sin y$.

In other words, the controlling equation of motion is articulated as follows:

$$y'' + c\,y' + a\,y + b\,y^2 - h\,y^3 + f \sin y = 0 \tag{2}$$

Equation (2) integrates linear, nonlinear, damping, and external forcing effects, rendering it appropriate for the analysis of complicated phenomena such as bifurcations, limit cycles, and chaotic dynamics in weakly nonlinear oscillators.

The nonlinear forces in Equation (2) can be categorized into three components: odd damping forces, quadratic nonlinear forces including quadratic damping, and the restoring force; thus, they can be expressed in terms of these components as follows:

$$y'' + f_1(y') + f_2(y) + f_3(y) = 0 \tag{3}$$

where $f_1(y')$ represents the linear damping force, $f_2(y)$ refers to the quadratic nonlinear Helmholtz function, and $f_3(y)$ indicates the cubic Duffing function. These functions are defined as follows:

$$\left.\begin{array}{c} f_1(y') = cy' \\ f_2(y) = by^2 \\ f_3(y) = ay + f \sin y \end{array}\right\} \tag{4}$$

The simplicity of He's formulation [20] can now be extended to derive analytical formulas for the total frequency of the damping Helmholtz–Rayleigh–DO.

Consider that the guesswork solution is provided by the following:

$$\widetilde{v} = B \cos \Omega t, \quad \text{ICs} \quad \widetilde{v}(0) = B, \quad \text{and} \quad \widetilde{v}'(0) = 0 \tag{5}$$

With the advantage of NPA, unlike all traditional perturbation methods, the weakness of relying on the Taylor expansion is unnecessary here.

To derive a straightforward and precise frequency–amplitude expression, the essentially equivalent linear oscillation ω_{eqv}^2 of Equation (3) can be articulated in relation to the nonlinear restoring force and the damping force σ_{eqv} as follows:

$$v'' + \sigma_{eqv} v' + \omega_{eqv}^2 v = 0 \tag{6}$$

It should be noted that the characteristic two parameters may be calculated as follows:

$$\sigma_{eqv} = \int_0^{2\pi/\Omega} \widetilde{v}' f_1(\widetilde{v}') dt \Big/ \int_0^{2\pi/\Omega} \widetilde{v}'^2 dt = c \tag{7}$$

and

$$\omega_{eqv}^2 = \int_0^{2\pi/\Omega} \widetilde{v} \left(\int_0^{\widetilde{v}} by^2 dy + f_3(\widetilde{v}) \right) dt \Big/ \int_0^{2\pi/\Omega} \widetilde{v}^2 dt = a + \frac{1}{4} B^2 (b - 3h) + \frac{2}{B} f J_1(B) \tag{8}$$

where $J_1(A)$ represents the Bessel function.

Within the framework of perturbation techniques, quadratic terms may be transformed into alternative odd terms via multiplication, division, integration, or differentiation. The implementation of NPA primarily relies on classifying odd functions arising from damping and other odd terms related to stiffness effects. The quadratic factors are incorporated to address damping or stiffness forces. There are two primary integrals: the first yields the equivalent damping, while the second pertains to the equivalent frequency. The integral of the even terms can be incorporated into either the primary integral or the alternate integral. The detailed methodology of NPA was elucidated and examined by the comprehensive works of El-Dib, who wrote numerous articles on the subject. We select solely two articles from El-Dib [20,21].

The previous integrals are combined to establish the total frequency Δ^2. In fact, the details of these integrals were previously given by El-Dib [20–22].

For more convenience, Equation (6) may be transformed to the standard simple harmonic motion as follows:

Set $v(t) = f'(t) Exp(-ct/2)$. Equation (6) then becomes the following:

$$f''(t) + \Omega^2 f(t) = 0 \tag{9}$$

where

$$\Omega^2 = a + \frac{1}{4} B^2 (b - 3h) + \frac{2}{B} f J_1(B) - \frac{1}{4} c^2 \tag{10}$$

Consider $\Omega^2 = \lambda^2$, where λ^2 signifies the right-hand side of Equation (10), which represents the transition curve; it follows that the stable region needs $\Omega^2 > \lambda^2$. Simultaneously, the unstable zone requires $\Omega^2 < \lambda^2$. For this purpose, consider an ordered pair (B, Ω^2) with some value of any other parameters. In fact, in the region of $\Omega^2 > \lambda^2$ with the solution of Equation (9), the trigonometric circular functions sin and cos are produced, which are bounded ones. Conversely, the areas beneath these transition curves indicate unstable settings $\Omega^2 < \lambda^2$. In this case, the governing ODE as given in Equation (9) gives the solutions of hypergeometric functions sinh and cosh, which are unbounded.

Therefore, to compromise stability, one obtains

$$a + \frac{1}{4} B^2 (b - 3h) + \frac{2}{B} f J_1(B) - \frac{1}{4} c^2 > 0 \tag{11}$$

For more convenience, a connection can be made for the selected sample system using MS between the preliminary nonlinear ODE, as stated in Equation (2), and the corresponding linear ODE, supplied in Equation (6); see Figure 2.

$$a = 2.0,\ b = 2.0,\ c = 0.1,\ h = 3.0,\ f = 1.0,\ \text{and}\ \ B = 0.1$$

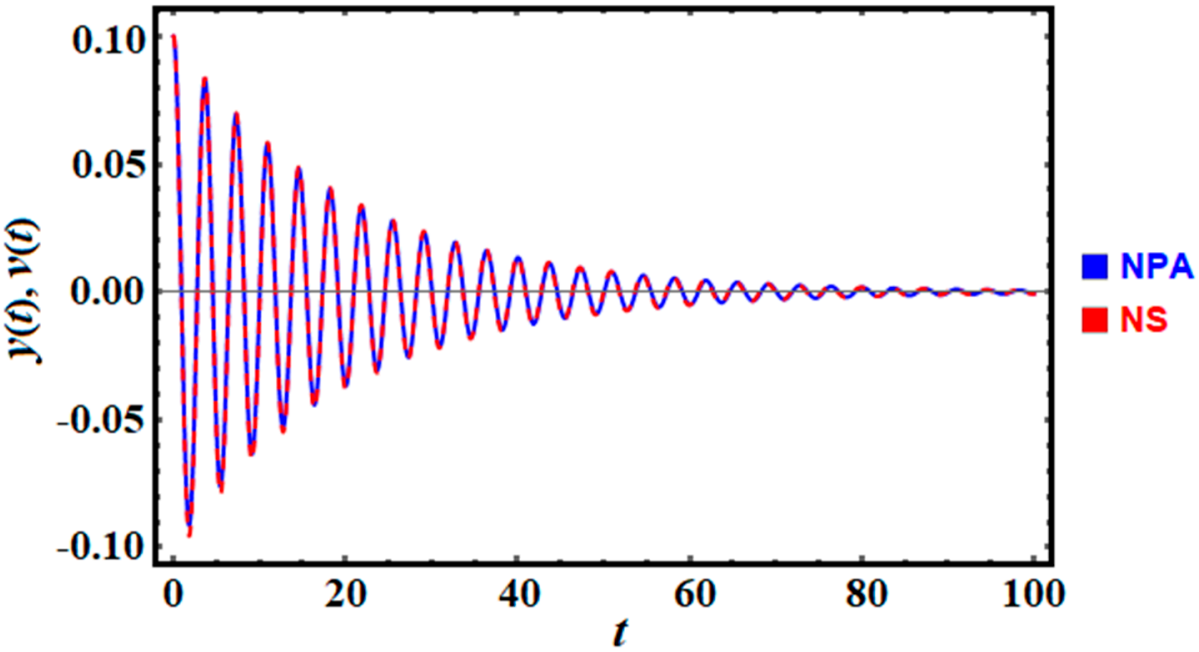


Figure 2. A good match between the two solutions of Equations (2) and (6).

A notable coincidence occurs between two plane oscillators, one is governed by a nonlinear ODE as presented in Equation (2) and the other is represented by a linear one as specified in Equation (6), when their trajectories in phase space or over time align remarkably, despite their fundamentally different mathematical structures. This transpires in specific conditions where the influence of nonlinearity is negligible or sufficiently mitigated by designated parameters, leading to a motion that closely approximates the linear case. In certain circumstances, a nonlinear system may exhibit harmonic or nearly harmonic oscillations with frequency and amplitude characteristics similar to those of its linear counterpart, suggesting a significant underlying symmetry within the nonlinear dynamics. Additionally, the MS computes the absolute error between the two solutions, providing an estimate of 0.00440857.

The obtained results are plotted for different values of the affected parameters, in which Figures 3 and 4 depict how the solution v oscillates and decays over time under varying parameter influences. Figure 3a–c shows how the solution v changes over time with different values of parameters a, b, and c, respectively. Each color in the graph represents a different parameter value. The graphs depict oscillations that decay over time, indicating damping effects in the system. Changes in parameter values appear to affect oscillation amplitude and decay rate. As the elastic restoring force's influence increases (red to black), the system's oscillations become quicker and more pronounced due to a stronger restoring force. The decay in amplitude over time indicates energy loss, likely due to damping. Greater values of b, which is a quadratic nonlinearity coefficient, lead to larger oscillation amplitudes initially, demonstrating a more prominent nonlinear effect on restoring force. As increasing c is related to damping, one can see that damping is more significant, leading to faster decay in oscillation amplitude.

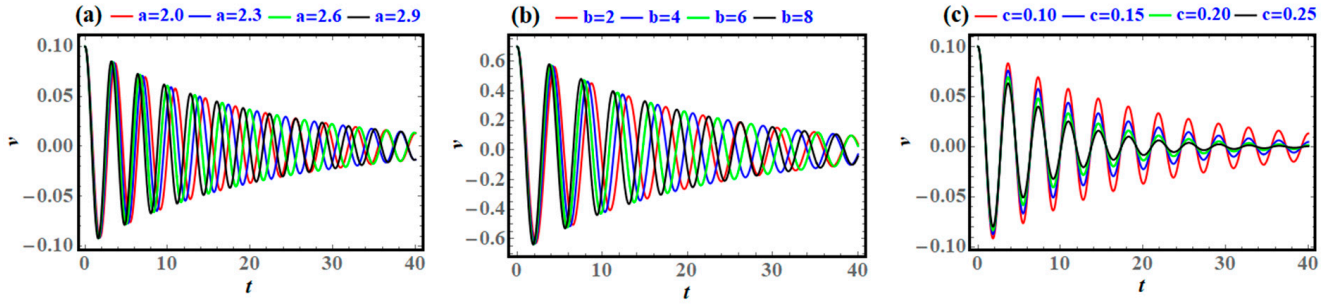


Figure 3. The behavior of $v(t)$ at various values of parameters a, b, and c.

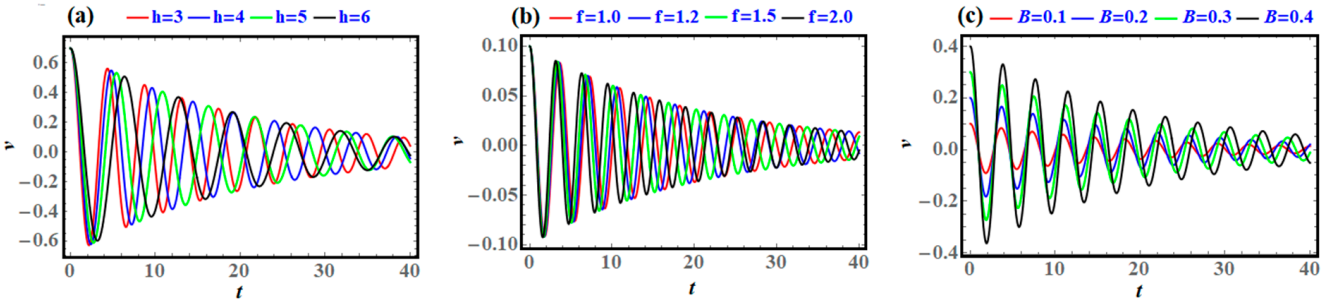


Figure 4. The behavior of $v(t)$ at various values of parameters h, f, and B.

Figure 4a–c is similar to Figure 3 but focuses on parameters h, f, and B. Again, variations in amplitude and oscillation decay are observed with changes in parameter values. Increasing h, which is associated with additional nonlinear terms, modifies the decay pattern and alters oscillation frequency, showcasing complex nonlinear dynamics. Larger f (represents external driving forces) values result in sustained oscillations, indicating the influence of external periodic forces. This reflects modifications in system dynamics due to external conditions or resistances according to the values of B, where higher B values change the amplitude and frequency of oscillations, suggesting alterations in the system's resistive forces.

The phase planes (v'' vs. v) are demonstrated in Figures 5 and 6, in which panels (a), (b), (c) of Figure 5 show phase portraits of different values of a, b, and c. The phase portraits are spiral patterns, indicating damping and stability in the system's trajectory towards a fixed point. Furthermore, panels (a), (b), (c) of Figure 6 illustrate phase portraits for parameters h, f, and B. Similar spiral trajectories are observed, providing insight into the system's behavior under damping and external restoring forces. In other words, spiral patterns indicate damping, as trajectories spiral inward towards a stable fixed point, showcasing energy loss over time. Different parameter values affect trajectory shape and convergence speed, revealing how system stability is affected by parameter changes. Tighter spirals represent faster energy dissipation, whereas broader spirals suggest lesser damping.

The stability curves are graphed in Panels (a), (b), (c), (d) of Figure 7 according to stability condition (11). Each panel in this figure shows stability regions in the Ω^2 vs. B plane for different values of a, b, h, and f. The graphs divide the plane into stable and unstable regions, with curves defining these areas. Changes in parameters shift the boundaries of stable and unstable regions, emphasizing the parameters' role in affecting stability. The color regions highlight how varying a parameter affects the width of the stability/instability zones. These diagrams depict regions of stability (where oscillations return to equilibrium) and instability (where oscillations grow unbounded).

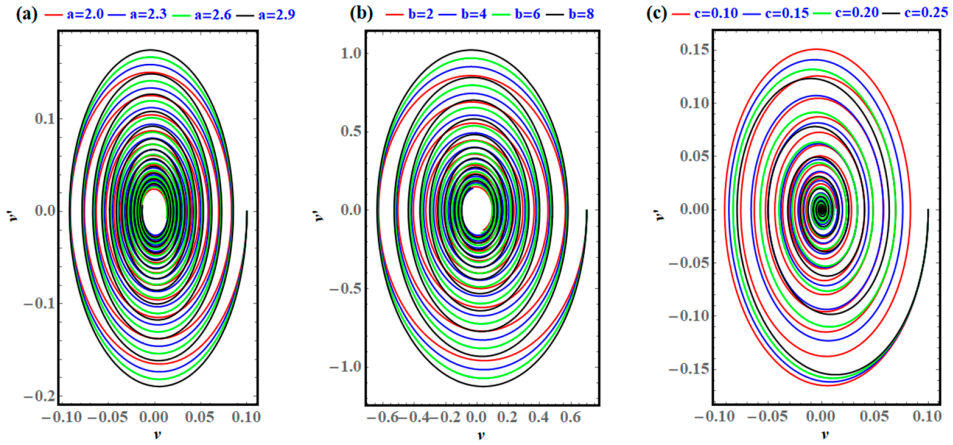


Figure 5. The corresponding phase plane diagrams of Figure 3 at the same values of the parameters considered.

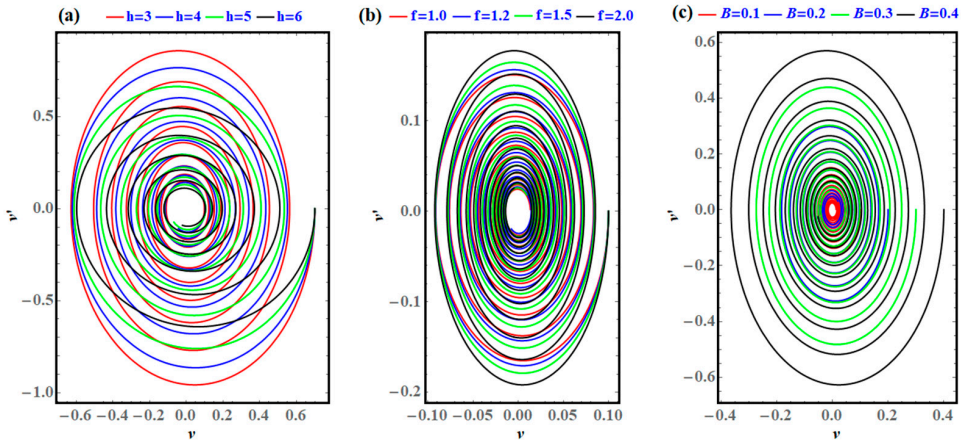


Figure 6. The corresponding phase plane diagrams of the considered values in Figure 4.

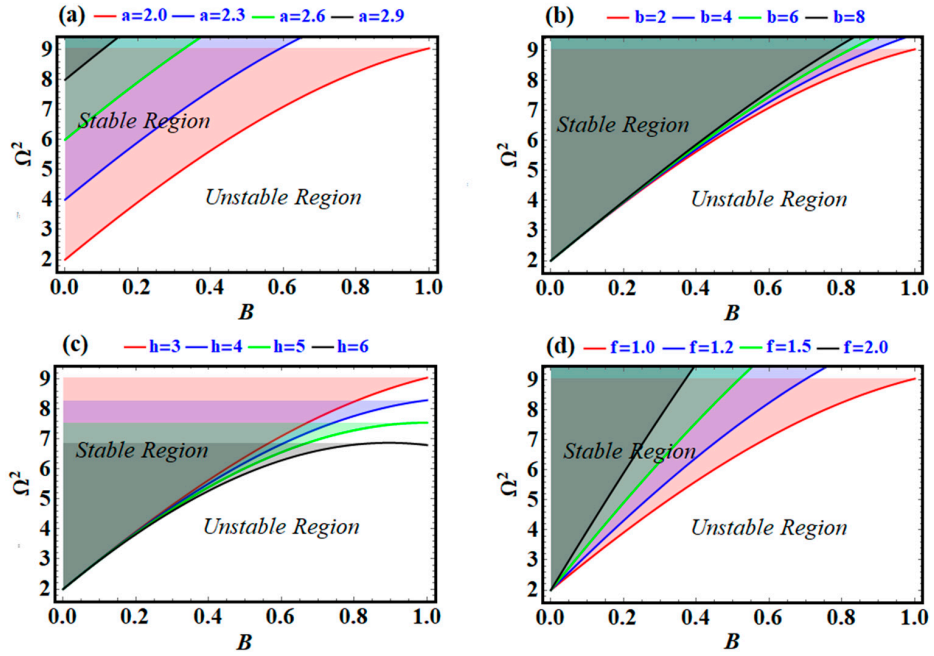


Figure 7. The stability regions at (**a**) $a(= 2.0, 2.3, 2.6, 2.9)$, (**b**) $b(= 2, 4, 6, 8)$, (**c**) $h(= 3, 4, 5, 6)$, and (**d**) $f(= 1.0, 1.2, 1.5, 2.0)$.

Overall, these figures illustrate the complex interplay between different forces in a damped harmonic oscillator system, highlighting how modifying system parameters can control oscillatory behavior and stability. This understanding is crucial in various engineering applications, such as designing stable mechanical structures or optimizing vibrating systems.

Investigation of System Dynamics via Chaos Assessments

The analysis of the dynamical system is conducted through a combination of BDs, PMs, and LEs of different parameter settings. These tools together provide a comprehensive picture of the system's stability, periodicity, and possible routes to chaos [22–27].

To analyze the BDs, let us consider Figures 8 and 9, which illustrate the variation in the maximum value of $y(t)$ as the parameter h increases from two to five of two distinct values of B (0.1 and 0.3, respectively). In both cases, the diagrams exhibit a single, stable horizontal branch, indicating that the maximum value of $y(t)$ remains constant throughout the explored range of h. The absence of branching or complex structure in the BDs suggests that, of these parameters, the system does not experience period doubling, chaos, or any bifurcation phenomenon. It remains in a stable, possibly periodic regime of all values of h considered, with $y(t)$ settling into constant amplitude.

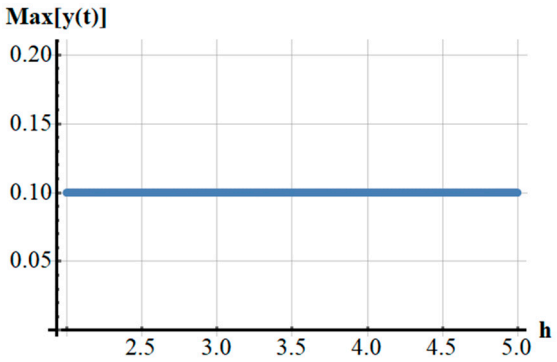


Figure 8. Bifurcation diagram as h varies (2 to 5); $B = 0.1$.

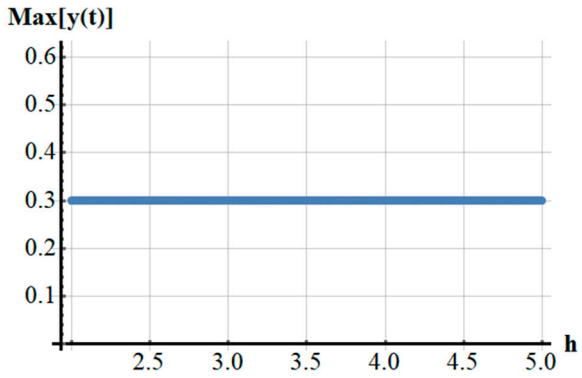


Figure 9. Bifurcation diagram as h varies (2 to 5); $B = 0.3$.

On the other side, Figures 10 and 11 display the Poincaré sections for $h = 3$ and two different values of B (0.1 and 0.3, respectively). In both cases, PMs reveal a concentrated cluster of points about the origin with only minor spread. These maps provide insights into the nature of the attractor in phase space. The clustering of points near the origin (with minor scatter due to numerical effects or weak perturbations) further supports the idea that the system exhibits regular, non-chaotic behavior. The maps lack the distributed, fractal-like structure that would be indicative of chaos. Furthermore, the slight increase in dispersion

for $B = 0.3$, as shown in Figure 11 compared to $B = 0.1$ and as plotted in Figure 10, hints at comparably greater sensitivity or excitation, though it remains very limited.

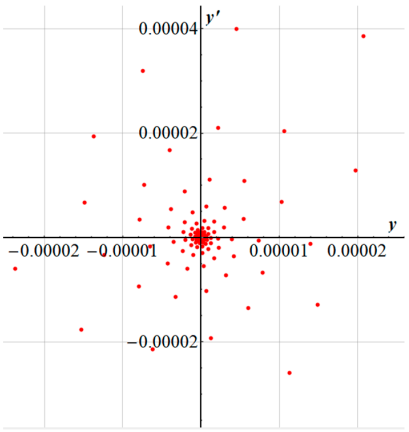


Figure 10. PM for $h = 3$; $B = 0.1$.

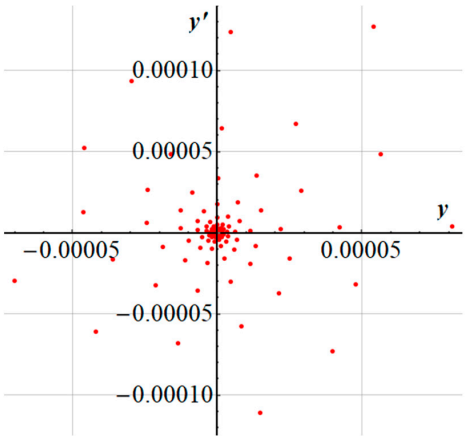


Figure 11. PM for $h = 3$; $B = 0.3$.

To validate the above analysis of the aforementioned model, let us consider LEs, as drawn in Figures 12 and 13. These figures display the two largest LEs (λ_1, and λ_2) as functions of h for both $B = 0.1$ and $B = 0.3$. In all cases, the exponents are negative and remain so over the entire range of h. The LE quantifies the average rate of divergence (or convergence) of nearby trajectories in the phase space. Negative values across the board indicate that all trajectories converge to a stable fixed point or limit cycle, confirming that the system does not exhibit chaos. The slight variation with h seen in both λ_1, and λ_2 for both values of B reflects some parametric sensitivity but does not alter the overall stability of the system.

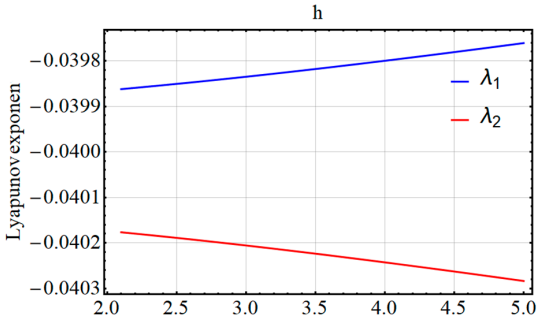


Figure 12. LEs when $a = b = 0.2, c = f = 0.1$, $B = 0.1$.

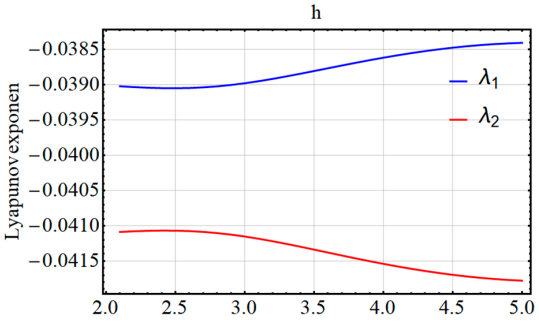


Figure 13. LEs when $a = b = 0.2, c = f = 0.1, B = 0.3$.

Based on this discussion, one can state the following notes: Taken together, the BDs, Poincaré sections, and LEs consistently indicate that the examined system operates in a stable, non-chaotic regime of the range of parameters explored ($h = 2$ to 5 and for both $B = 0.1,$ and $B = 0.3$). No evidence of bifurcation, period doubling, or transition to chaos is observed. The system essentially trends towards a periodic or steady-state solution, which is robust against the moderate changes in the parameters tested. This comprehensive stability is further underscored by the tightly negative Lyapunov spectra and concentrated Poincaré points, supporting the notion of regular, well-behaved dynamics within the chosen parameter space. Therefore, one can anticipate the predictable and repeatable system behavior of these parameter values, with minimal risk of chaotic divergence.

2.2. The Second Application

The second application can be considered as a cylindrical surface with a horizontal axis and radius R, centered at the point 0. This cylinder is fixed. Inside it, there is a swinging longitudinal sector of a homogeneous solid cylinder of radius r. As shown in Figure 14, its projection appears as a symmetrical circular sector. The rolling occurs without slipping. The line connecting two centers A, and C make an angle θ with the vertical line, while making an angle ϕ with the axis of symmetry of the circular sector. The weight of the circular sector is mg, passing through the center of the uniform rolling sector C. The angle between the axis of symmetry of the given sector and the vertical line is β. The angular velocity of the sector is the rate of change in the angle β with respect to time t. Here, the motion is considered as a planar motion with a single degree of freedom. We aim to derive the equation of motion and then analyze it.

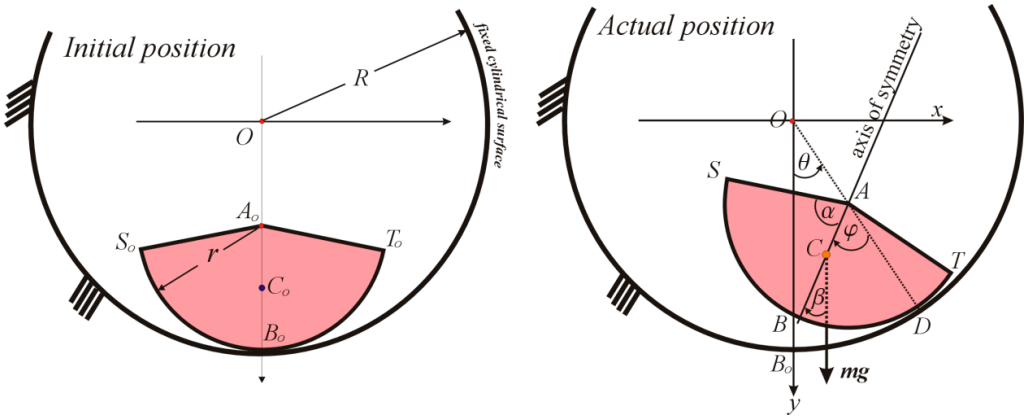


Figure 14. The initial and actual position of an oscillating sector on the internal surface of a fixed cylinder.

From the indicated Figure 14, it can be easily stated that the coordinates of $C(x_c, y_c)$ may be represented as follows:

$$\begin{cases} x_C = (R-r)\sin\theta - q\sin\left(\frac{R-r}{r}\theta\right), \\ y_C = (R-r)\cos\theta - q\cos\left(\frac{R-r}{r}\theta\right), \end{cases} \tag{12}$$

where $q = \frac{2r}{3}\frac{\sin\alpha}{\alpha}$.

The kinetic energy Q of the vibrating circular sector can be derived as follows:

$$Q = \frac{m}{2}\dot{\theta}^2\left(\frac{3}{2}(R-r)^2 - \frac{2q}{r}(R-r)^2\cos(R\theta/r)\right). \tag{13}$$

The potential energy P of the vibrating circular sector may be written as follows:

$$P = -mg\left((R-r)\cos\theta + q\cos(\frac{R-r}{r}\theta)\right). \tag{14}$$

Finally, the governing equation of motion may be written as follows:

$$\varphi'' + \frac{8}{9}\beta\varphi''\cos\varphi + \frac{1}{4}\beta\varphi'^2\sin\varphi + \frac{2}{3}K\sin((1+1/\beta)\,\varphi) + \frac{4}{9}K\beta\sin(\varphi/\beta) = 0, \tag{15}$$

where $\beta = \sin\alpha/\alpha$, and $K = R/(R-r)$.

The ICs are represented as follows:

$$\varphi(0) = D, \text{ and } \varphi'(0) = 0 \tag{16}$$

Equation (15) may be formulated as follows:

$$\varphi'' + G(\varphi, \varphi'') = 0 \tag{17}$$

where $G(\varphi, \varphi'') = \frac{8}{9}\beta\varphi''\cos\varphi + \frac{1}{4}\beta\varphi'^2\sin\varphi + \frac{2}{3}K\sin((1+1/\beta)\varphi) + \frac{4}{9}K\,\beta\sin(\varphi/\beta)$.

The trial (guessing) solution may be represented as follows:

$$\eta = D\cos\Sigma t \tag{18}$$

where Σ is the total frequency, which will be established later.

As previously mentioned, the following equations are similar to Equations (7) and (8). With similar ICs as given in Equation (16), using the disadvantage of Taylor expansion is not necessary in this situation due to the advantages of NPA despite all other standard perturbation techniques. Since there are no damping terms, by making use of MS, it follows that the total frequency could be determined as follows, as demonstrated by Moatimid et al. [17–19]:

$$\Sigma^2 = \frac{-32\beta\Sigma^2 J_1(D) + 24KJ_1\left(\frac{D}{\beta}\right) + D(9+32\beta)\Sigma^2 J_2(D)}{18D} \tag{19}$$

Solve Equation (19) to find an expression for the total frequency as follows:

$$\Sigma^2 = \frac{24KJ_1\left(\frac{D}{\beta}(1+\beta)\right)}{32\beta J_1(D) + D(18-(9-32\beta)J_2(D))} \tag{20}$$

Now, the comparable linear ODE may be formulated as follows:

$$\eta'' + \Sigma^2\eta = 0 \tag{21}$$

The stability standard necessitates

$$\frac{24KJ_1\left(\frac{D}{\beta}(1+\beta)\right)}{32\beta J_1(D)+D(18-(9-32\beta)J_2(D))}>0 \tag{22}$$

For better ease, the nonlinear ODE as provided in Equation (15) can be matched with the linear comparative ODE as given in Equation (21), using MS via the command NDsolve; see Figure 15. Select a dynamical system from the data set:

$$\alpha=\pi/6,\ R=3.0;\ r=1.0,\ \text{and}\ \ D=0.5$$

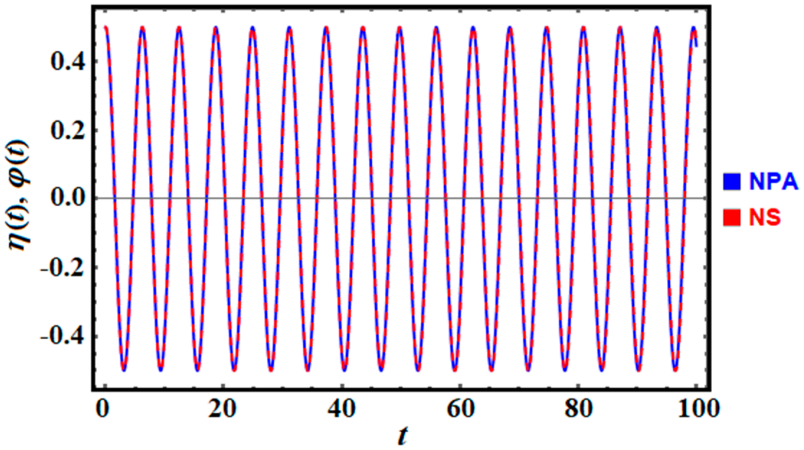


Figure 15. A match between the linear Equation (17) and the nonlinear ODE as given in Equation (21).

A notable coincidence occurs between the two plane oscillators, one governed by a nonlinear ODE as specified in Equation (17) and the other by a linear ODE as shown in Equation (21), when their trajectories in phase space or over time align distinctly, despite their fundamentally different mathematical structures. This emerges under defined conditions where the influence of nonlinearity is negligible or sufficiently regulated by specific parameters, leading to a motion that nearly mirrors the linear scenario. Under some situations, the nonlinear system may exhibit harmonic or nearly harmonic oscillations with frequency and amplitude characteristics similar to those of its linear counterpart, suggesting a significant underlying symmetry within the nonlinear dynamics. The MS computes the absolute error between the two solutions, resulting in a number of 0.0392802.

In what follows, we are going to examine the graphical representations of the obtained results of the present system. Figure 16a–c presents the time histories of the solution $\eta = D\cos\Sigma t$ at various values of β, K, and D, where $K = R/(R-r)$, and $D = \phi(0)$. The corresponding phase plane plots are represented in parts of Figure 17 for the same values of β, K and D. The stability and instability areas are graphed in Figure 18a,b when β, and K have different values.

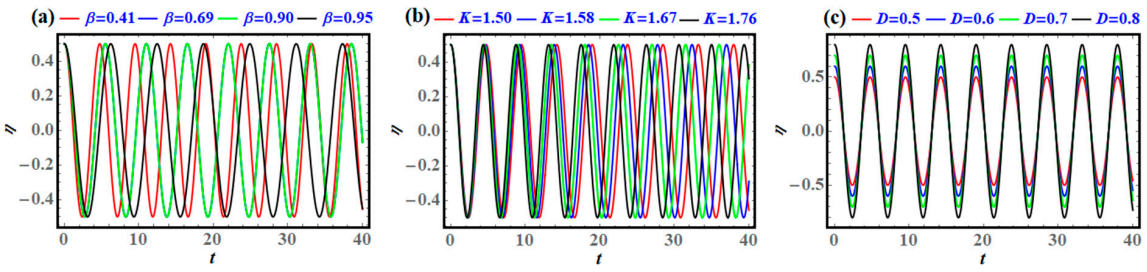


Figure 16. The time–behavior of solution η at various values of (**a**) $\beta(=\ 0.41, 0.69, 0.90, 0.95)$, (**b**) $K(=1.5, 1.58, 1.67, 1.76)$, and (**c**) $D(=0.5, 0.6, 0.7, 0.8)$.

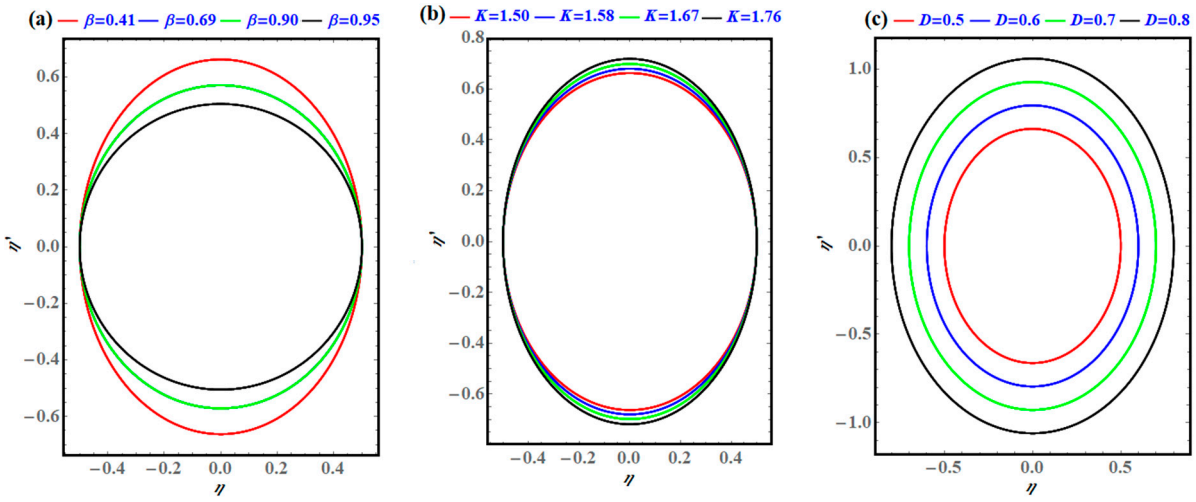


Figure 17. The corresponding phase plane diagrams of the considered values in Figure 16.

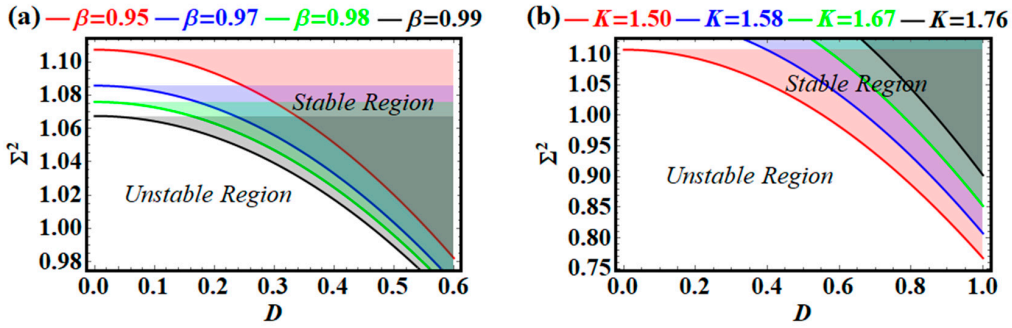


Figure 18. The stability areas in view of the condition (19) at (**a**) $\beta(= 0.95, 0.97, 0.98, 0.99)$ and (**b**) $K(= 1.5, 1.58, 1.67, 1.76)$.

Let us provide a more in-depth description and physical analysis of the presentation in Figures 16–18. The behavior of motion can be described as the sector rolling back and forth (oscillates) about the lowest energy point. The curvature and mass affect how "stiff" or "floppy" the restoring torque is. Rolling without slipping means kinetic and potential energy constantly exchange.

The time histories are graphed in portions (Figure 16a–c) for various values of the impacted parameters. The influence of these parameters can be interpreted as follows: Each parameter shows how the oscillation η (suitably scaled angle) varies in the time of a different fixed β. Oscillation becomes faster as β increases due to β likely parameterizing how "upright" the rolling wedge is inside the shell in equilibrium. When the center of mass is higher (larger β), the lever arm for gravity, the restoring torque, becomes longer, so the force pulling it back to the middle is greater. Consequently, rocking becomes "stiffer," and the frequency increases. The other side effect of K (measure how much space between the shell and the rolling sector) can be demonstrated as follows: higher K (which happens when the inner sector is much smaller than the shell) means more cycles in a fixed time, which means frequency increases. As K increases, the sector travels further per rotation, but since it is smaller, it is easier to tip and "falls" back more quickly. The restoring geometry is stronger relative to the mass moment of inertia. The amplitude of oscillation increases with D, but the period (time for one cycle) does not change. This matches the simple harmonic oscillator: energy is proportional to how far you displace the system, but the intrinsic frequency is set by system parameters (β, K), not by amplitude for small oscillations.

The phase plane curves are graphed in Figure 17a–c (Plotting η' vs. η). Each trajectory is an ellipse (or nearly so), showing the exchange of kinetic and potential energy. The area

inside each loop is proportional to the total energy of motion. For D, loops become bigger (more displacement = more energy). For K and β, loop width/height may change due to frequency/energy change or may be subtle (depending on how the parameter scales into kinetic or potential terms). The interpretation of these curves can be stated as follows: If the system is stable, it traces closed ellipses (bounded energy, oscillating forever). If initial conditions or parameters cross a threshold, you will see spiraling out (not shown here, but would be seen for instability).

The stability diagrams are graphed in Figure 18, in which Σ^2 (a frequency) versus the initial displacement D is presented. Above each curve, the areas are stable (oscillations will always remain bounded, no matter the initial push), while below each curve, the unstable regions are noticed (small disturbance grows without bound; possible "flip-over" of sector). For increasing β (panel a), the stability zone becomes larger. You can rock farther or have a more upright sector without losing control. For increasing K (panel b), the stability threshold climbs. With larger K (smaller sector), it is easier to destabilize the system, so you must keep Σ^2 higher for the same safe region. The stability diagrams are like safe operating charts: for the given geometry and initial displacement, you can predict whether the oscillator will settle down or tip over and can design safe parameters accordingly.

The dynamic and stability properties of the rocking–rolling sector system are most favorably controlled by maximizing uprightness β, minimizing the sector-to-shell size mismatch K, and limiting initial displacement D. Stable oscillations are achievable in wider physical and operational ranges with higher β and lower K, while large values of D or K, or a poorly chosen β, increase the system's susceptibility to instability. These insights are keys of engineering design, allowing you to predict safe working ranges for such rolling–oscillatory systems and prevent mechanical failures due to run-away instability.

Discussion of BDs, PMs, and LEs

To examine the complex dynamics of the system as the parameter R varies, we utilize BD, PM, and LE analysis. These methods together provide insights into the onset of periodicity, quasi-periodicity, and potential of chaotic behavior.

Figures 19 and 20 present BDs of the system as R that varies from 3.0 to 5.0, with $r = 1.0$, as seen in Figure 19 and $r = 2.4$, and as plotted in Figure 20. In both cases, the diagrams clearly reveal the emergence of bifurcations and a progression toward increasingly complex dynamic regimes. As R increases, the system transitions from a state of relatively simple behavior (single or few points of each value of R) to states exhibiting multiple branches and dense clouds of points. Because variations in R do not produce a noticeable change in the function ϕ which remains very close to zero, the system's dynamics tend to be non-chaotic, i.e., stable.

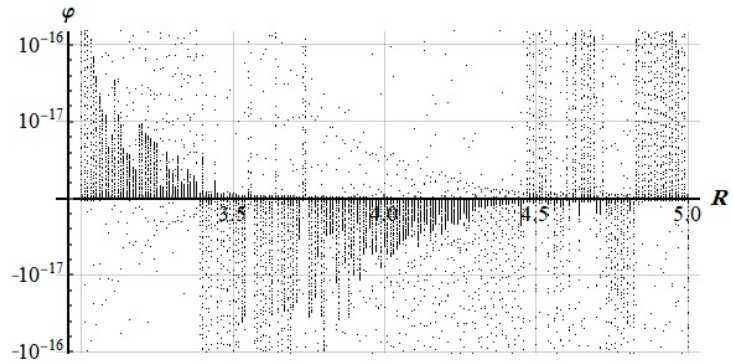


Figure 19. Bifurcation diagram as R varies (3 to 5); $r = 1$.

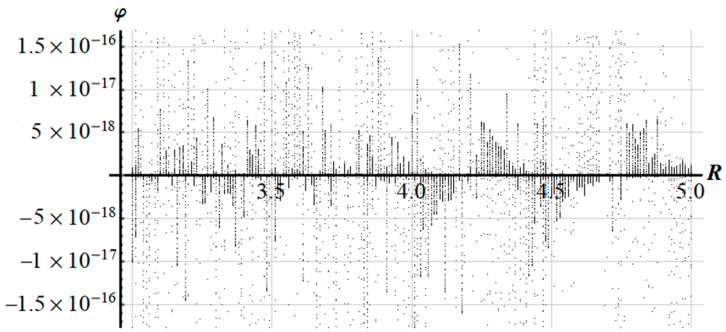


Figure 20. Bifurcation diagram as R varies (3 to 5); $r = 2.4$.

Further insights into the nature of the system's attractors can be found in the Poincaré sections as displayed in Figures 21 and 22. The map of $R = 2.5$ (Figure 21) displays a series of closed loops, indicative of a regular, possibly periodic or quasi-periodic orbit. By contrast, when R increases to 3.5 (Figure 22), the PM reveals a more dispersed pattern with less regular structure, suggesting that the system's dynamics have become more complex, possibly entering a state of quasi-periodicity or even weak chaos. The shift from recognizable loops to a more scattered point distribution in the map reflects the system's increased sensitivity to initial conditions, a hallmark of chaotic dynamics.

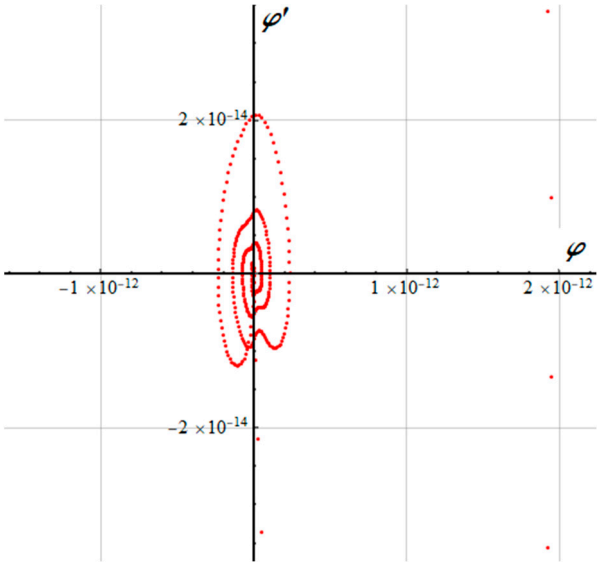


Figure 21. PM for $R = 2.5$.

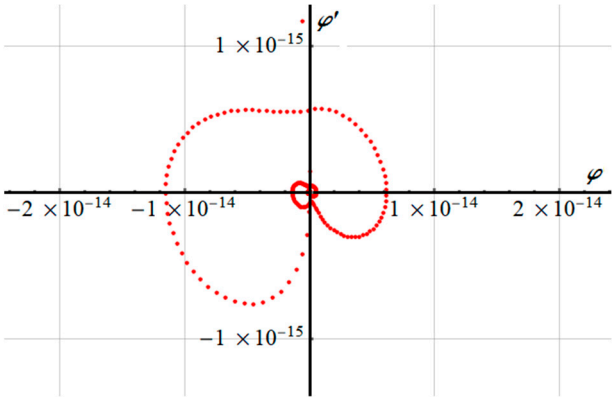


Figure 22. PM for $R = 3.5$.

The LEs, shown in Figures 23 and 24, provide a quantitative measure of the system's sensitivity to initial conditions. For both parameter sets ($r = 0.1$ in Figure 23 and $r = 2.4$ in Figure 24), λ_1 (blue curve) remains near or below zero across the full range of R, while λ_2 (red curve) is distinctly negative. These results suggest that even as the system exhibits increasingly complex motion in the bifurcation and Poincaré analyses, it does not fully enter a chaotic regime within the examined parameter range, since a positive LE, an unequivocal indicator of chaos, is not observed. The consistently negative values instead point towards stable or quasi-periodic behavior, where trajectories do not diverge exponentially from each other.

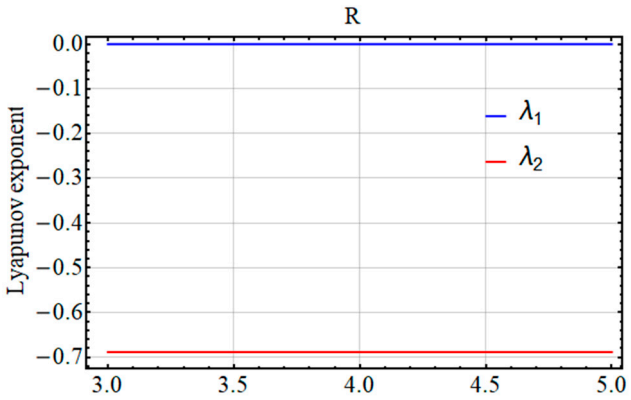


Figure 23. Shows LEs when $\alpha = \pi/5, r = 0.1,\ d = 0.6$.

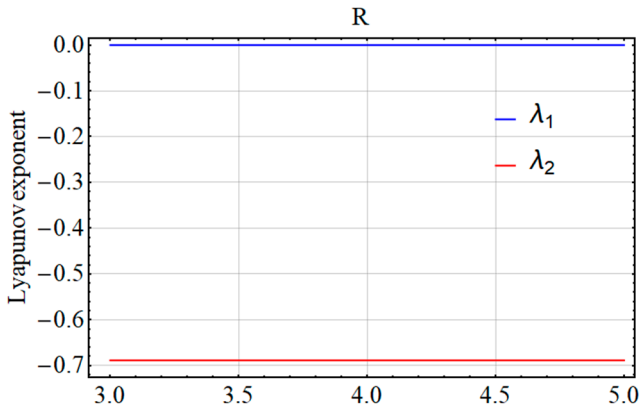


Figure 24. LEs at $\alpha = \pi/5, r = 2.4,\ d = 0.6$.

In view of the above analysis of Figures 19–24, the combined analysis via BDs, PMs, and LEs illustrates how increasing R and altering r can drive the system from regular periodic behavior towards more intricate dynamics with a higher degree of sensitivity. However, the lack of a positive LE suggests that while the system may approach chaos (as shown by the denser and more fragmented bifurcation and Poincaré plots), it remains bounded within stable or quasi-periodic dynamics for the given ranges of parameters. This multi-faceted examination underscores the richness of nonlinear dynamical systems, where transitions to complexity manifest in both qualitative and quantitative diagnostics.

3. Concluding Remarks

The innovative methodology signified a pivotal transformation in the examination and comprehension of complex systems, departing beyond the incremental modifications characteristic of traditional perturbation approaches. The NPA directly confronted the intrinsic complexities and nonlinearities of these systems. The link between frequency and amplitude was essential in understanding the dynamics of oscillatory systems and

regulating their behavioral patterns and responses. The study examined the intricacies of the frequency amplitude formula, highlighting its essential function in both linear and nonlinear oscillatory scenarios. As a depth investigation highlighted the formula's crucial role in forecasting system behavior, particularly in situations with varying amplitudes. The results emphasized the formula's efficacy as a potent tool of advanced system characterization, with significant implications across diverse scientific and engineering domains. This research broadened the formulation of the frequency–amplitude relationship beyond conventional cubic dependencies of the restoring force. A formula for determining the frequency of individual oscillators was introduced. The methodology, characterized by its simplicity, served as a powerful analytical instrument for the investigation of highly nonlinear vibrations, promoting a more sophisticated and comprehensive examination of vibrational events. The system's dynamics are examined via chaotic evaluations, employing BDs, PMs, and LEs. This study outlines the shifts between regular and complicated behavior and thoroughly assesses the stability features of the system. The findings yield a thorough comprehension of the fundamental nonlinear dynamics and furnish significant insights for forthcoming investigations into analogous systems. The principal key outcomes can be summarized as follows:

The NPA in analyzing coupled weakly nonlinear oscillators addresses the shortcomings of classical perturbation methods, particularly near resonances and in strongly coupled scenarios. It offers a unified approach that accurately depicts nonlinear interactions without small-parameter expansions, enhancing the understanding of bifurcations, energy exchanges, and chaos. This method provides insights into complex dynamical phenomena often inadequately approximated by traditional perturbation techniques.

The examination of coupled nonlinear ODEs is crucial, as numerous real-world systems comprise interacting components whose actions intricately affect each other in nonlinear manners. These models are crucial in comprehending collective dynamics, synchronization, feedback processes, and emergent phenomena across disciplines like physics, biology, engineering, ecology, and social sciences. Examining coupled nonlinear ODEs allows researchers to understand realistic system interactions, forecast multi-variable progression across time, and formulate effective strategies for control, optimization, and stability in interconnected systems.

Author Contributions: G.M.M.: conceptualization, resources, methodology, formal analysis, validation, visualization, writing—original draft preparation, reviewing. T.S.A.: investigation, validation, methodology, data duration, conceptualization, reviewing. A.A.G.: conceptualization, formal analysis, validation, data duration, software, reviewing and editing. All authors have read and agreed to the published version of the manuscript.

Funding: This research received no external funding.

Data Availability Statement: All data generated or analyzed during this study are included in this published article.

Conflicts of Interest: The authors state that there are no conflicts of interest associated with this work.

References

1. Liu, Y.; Guo, S.; Wang, T.; Jin, H. An effective evaluation framework for security systems using ordinary differential equations. *Adv. Contin. Discret. Models* **2026**, *2026*, 13. [CrossRef]
2. Cao, H.; Khan, K.A. A kinematic smoothing method for tightening convex relaxations of ordinary differential equations. *J. Glob. Optim.* **2026**, *94*, 65–93. [CrossRef]
3. Alsharidi, A.K.; Muhib, A. Oscillatory behavior for higher-order nonlinear differential equations in the canonical case. *Alsharidi Muhib J. Inequalities Appl.* **2026**, *2026*, 18. [CrossRef]

4. Biçer, E.; Tunç, C. On the asymptotic stability behaviours of solutions of non-linear differential equations with multiple variable advanced arguments. *J. Appl. Nonlinear Dyn.* **2019**, *8*, 239–249. [CrossRef]
5. Ismail, G.M.; Abul-Ez, M.; Zayed, M.; Farea, N.M. Analytical accurate solutions of nonlinear oscillator systems via coupled homotopy-variational approach. *Alex. Eng. J.* **2022**, *61*, 5051–5058. [CrossRef]
6. Kopmaz, O. Free vibrations of a mass grounded by linear and non-linear springs in series. *J. Sound Vib.* **2006**, *289*, 689–710.
7. Manimegalai, K.; Sagar Zephania, C.F.; Bera, P.K.; Bera, P.; Das, S.K.; Sil, T. Study of strongly nonlinear oscillators using the Aboodh transform and the homotopy perturbation method. *Eur. Phys. J. Plus* **2019**, *134*, 462. [CrossRef]
8. Abu-As'ad, A.; Asad, J. Power series approach to nonlinear oscillators. *J. Low Freq. Noise Vib. Act. Control.* **2023**, *43*, 220–238. [CrossRef]
9. Shou, D.-H. The homotopy perturbation method for nonlinear oscillators. *Comput. Math. Appl.* **2009**, *58*, 2456–2459. [CrossRef]
10. Hermann, M.; Saravi, M.; Khah, H.E. Analytical study of nonlinear oscillatory systems using the Hamiltonian approach technique. *J. Theor. Appl. Phys.* **2014**, *8*, 133. [CrossRef]
11. Ismail, G.M. An analytical coupled homotopy-variational approach for solving strongly nonlinear differential equation. *J. Egypt. Math. Soc.* **2017**, *25*, 434–437. [CrossRef]
12. Ismail, G.M.; Abu-Zinadah, H. Analytic approximations to non-linear third order Jerk equations via modified global error minimization method. *J. King Saud Univ.—Sci.* **2021**, *33*, 101219. [CrossRef]
13. He, J.H. Some asymptotic methods for strongly nonlinear equations. *Int. J. Mod. Phys. B* **2006**, *20*, 1141–1199. [CrossRef]
14. He, J.-H. The simpler, the better: Analytical methods for nonlinear oscillators and fractional oscillators. *J. Low Freq. Noise Vib. Act. Control.* **2019**, *38*, 1252–1260. [CrossRef]
15. Qie, N.; Hou, W.F.; He, J.-H. The fastest insight into the large amplitude vibration of a string. *Rep. Mech. Eng.* **2020**, *2*, 1–5. [CrossRef]
16. He, J.-H.; Yang, Q.; He, C.-H.; Khan, Y. A simple frequency formulation for the tangent oscillator. *Axioms* **2021**, *10*, 320. [CrossRef]
17. Alluhydan, K.; Moatimid, G.M.; Amer, T.S.; Galal, A.A. A Novel Inspection of a Time-Delayed Rolling of a Rigid Rod. *Eur. J. Pure Appl. Math.* **2024**, *17*, 2878–2897.
18. Alanazy, A.; Moatimid, G.M.; Amer, T.S.; Galal, A.A. Non-Perturbative Approach in Scrutinizing Nonlinear Time-Delay of Van der Pol-Duffing Oscillator. *Eur. J. Pure Appl. Math.* **2025**, *18*, 5495.
19. Moatimid, G.M.; Amer, T.S.; Galal, A.A. An innovative methodology in analyzing certain pendulum oscillators. *Sci. Rep.* **2025**, *15*, 15883. [CrossRef]
20. El-Dib, Y.O. Insightful and comprehensive formularization of frequency–amplitude formula for strong or singular nonlinear oscillators. *J. Low Freq. Noise Vib. Act. Control.* **2023**, *42*, 89–109. [CrossRef]
21. El-Dib, Y.O. A review of the frequency-amplitude formula for nonlinear oscillators and its advancements. *J. Low Freq. Noise Vib. Act. Control.* **2024**, *43*, 1032–1064. [CrossRef]
22. El-Dib, Y.O.; Elgazery, N.S. Periodic solution of the parametric Gaylord's oscillator with a non-perturbative approach. *Europhys. Lett.* **2022**, *140*, 52001. [CrossRef]
23. Amer, T.S.; Moatimid, G.M.; Zakria, S.K.; Galal, A.A. Dynamical analysis of a four-degree-of-freedom vibratory structure: Bifurcation, stability, and resonance exploration. *J. Low Freq. Noise Vib. Act. Control.* **2025**, *44*, 1555–1575. [CrossRef]
24. Khan, A.; Li, C.; Zhang, X.; Cen, X. Two-Memristor-based Chaotic System with Symmetric Bifurcation and Multistability. *Chaos Fractals* **2025**, *2*, 1–7. [CrossRef]
25. Uddin, M.J.; Santra, P.K.; Rana, S.M.S.; Mahapatra, G.S. Chaotic Dynamics of the Fractional Order Predator-Prey Model Incorporating Gompertz Growth on Prey with Ivlev Functional Response. *Chaos Theory Appl.* **2024**, *6*, 192–204. [CrossRef]
26. Bouali, S. Partial prey migration as a non-autonomous harmonic oscillator: Chaos-order transitions in a forced classical lotka-volterra model. *Chaos Fractals* **2025**, *2*, 50–58. [CrossRef]
27. Sarbinowski, F.; Awrejcewicz, J.; Grzelczyk, D. Bifurcations, Multistability, and Synchronization in the 7-DOF Electromechanical Stick–Slip System. *Machines* **2025**, *13*, 1082. [CrossRef]

Disclaimer/Publisher's Note: The statements, opinions and data contained in all publications are solely those of the individual author(s) and contributor(s) and not of MDPI and/or the editor(s). MDPI and/or the editor(s) disclaim responsibility for any injury to people or property resulting from any ideas, methods, instructions or products referred to in the content.